



University  
of Glasgow

Robb, P.D., Finnie, M., and Craven, A.J. (2012) Characterisation of InAs/GaAs short period superlattices using column ratio mapping in aberration-corrected scanning transmission electron microscopy. *Micron*, 43 (10). pp. 1068-1072. ISSN 0968-4328

<http://eprints.gla.ac.uk/66656>

Deposited on: 29 June 2012

# Characterisation of InAs/GaAs short period superlattices using column ratio mapping in aberration-corrected scanning transmission electron microscopy

Paul D. Robb<sup>1,2\*</sup>, Michael Finnie<sup>1</sup>, Alan J. Craven<sup>1,2</sup>

<sup>1</sup>SUPA School of Physics & Astronomy, University of Glasgow, G12 8QQ, UK

<sup>2</sup>SuperSTEM Laboratory, Daresbury Laboratory, WA4 4AD, UK

*\*Correspondence:* Room 402  
Department of Physics and Astronomy  
University of Glasgow  
Glasgow G12 8QQ  
paul\_robb@live.co.uk

## Abstract

The image processing technique of column ratio mapping was applied to aberration-corrected high angle annular dark field (HAADF) images of short period MBE (molecular beam epitaxy) grown InAs/GaAs superlattices. This method allowed the Indium distribution to be mapped and a more detailed assessment of interfacial quality to be made. Frozen-phonon multislice simulations were also employed to provide a better understanding of the experimental column ratio values. It was established that ultra-thin InAs/GaAs layers can be grown sufficiently well by MBE. This is despite the fact that the Indium segregated over 3-4 monolayers. Furthermore, the effect of the growth temperature on the quality of the layers was also investigated. It was demonstrated that the higher growth temperature resulted in a better quality superlattice structure.

**Keywords:** HAADF imaging; InAs/GaAs superlattices; column ratio mapping; Indium segregation

## 1. Introduction

III-V heterostructures are important for the fabrication of advanced optoelectronic and microelectronic devices such as high electron mobility transistors (Davies, 2005; DiLorenzo et al., 1997; Fu et al., 2008; Malmkvist et al., 2006; Sze, 2002). The In(Ga)As/GaAs system offers the prospect of improved electrical properties including higher carrier mobility and narrower band gaps. The realisation of high-performance devices depends on flat and abrupt heterointerfaces and high crystal quality. Molecular beam epitaxy (MBE) is one technique that is often utilised to grow such structures to the accuracy of a few atomic layers (Cheng, 1997). Previous studies have shown that In(Ga)As/GaAs multilayers can be successfully constructed from relatively wide layers on the order of several nanometres (Kitada et al., 2007; Noda et al., 2005; Rebohle et al., 2003). Nevertheless, it has been recognised that In(Ga)As based structures are difficult to grow to the same quality as equivalent AlAs/GaAs based structures (Howe et al., 2005; Karpov and Makarov, 2000). This is due to the surface segregation of the In atoms over several monolayers (ML) during the growth process. Hence, InAs/GaAs layers lack compositional abruptness and exhibit significant interface roughness.

Several characterisation methods have been used to study the In(Ga)As/GaAs system. These include photoluminescence, reflection high-energy electron diffraction, X-ray photoemission spectroscopy, scanning tunnelling microscopy and scanning transmission electron microscopy (STEM) (Eisele et al., 2003; Huang et al., 2004; Mozume and Gozu, 2009). With the advent of aberration-corrected STEM instruments, it is now commonplace to resolve the positions of individual atomic columns (Klenov and Stemmer, 2006). High angle annular dark field (HAADF) STEM imaging is typically employed to give atomic number (Z) contrast images due to the collection of Rutherford-like scattering (Pennycook and Jesson, 1991, 1990). In a qualitative model of HAADF image contrast, high-spatial resolution information is given by atomic column intensities that are associated with probe channelling (Dwyer and Etheridge, 2003; Hillyard et al., 1993; Rossouw, 2003). In comparison, the underlying background signal is generated by the average scattering from the de-channelled probe and therefore provides non-local information about the specimen.

For HAADF images of [001] grown III-V semiconductors viewed along the  $\langle 110 \rangle$  direction, interfacial quality can be evaluated by examining the change in the dumbbell column ratio across the layers. This is defined as the ratio of the Group III and Group V column intensities

for each dumbbell. The level of sharpness is then defined by the distance over which the column ratio switches in value across the boundary. The processing technique of column ratio mapping was developed for  $\langle 110 \rangle$  oriented III-V semiconductors (Robb and Craven, 2008; Robb et al., 2012). This automated procedure separates the high-spatial resolution information from the background signal and provides an objective and consistent measurement of the column ratio of all of the dumbbells in an image. In this way, a high-resolution HAADF image is converted into a column ratio map thereby allowing the local compositional variation to be observed without the confounding background signal.

In this paper, column ratio mapping is applied to ultra-thin short period MBE grown InAs/GaAs superlattices to demonstrate how layer quality and the degree of In diffusion can be explored through the use of aberration-corrected HAADF imaging. The first superlattice studied is composed of 6 repeat units of 1ML InAs/6ML GaAs and the second is composed of 10 repeat units of 1ML InAs/3ML GaAs. The effect of growth temperature on the quality of the layers is also considered by growing the second structure twice at different temperatures. In addition, frozen-phonon multislice calculations of the column ratio of bulk InAs and bulk GaAs are provided as a function of specimen thickness to improve the interpretation of the measurements. Moreover, the simulated GaAs values are compared to experimental values to gauge the accuracy of the simulations. Simulations across a perfect InAs/GaAs interface are also provided to demonstrate that any observed changes in column ratio values are due to compositional mixing and not simply the result of probe spreading across an ideal interface.

## **2. Experiment and simulation details**

The 1ML InAs/6ML GaAs superlattice was grown on a bulk GaAs wafer along the [001] crystal direction by MBE. No wafer rotation was employed during the growth process and the superlattice was grown at a substrate temperature of 575°C. Two versions of the 1ML InAs/3ML GaAs superlattice were grown on the same GaAs wafer. The first was grown in a similar fashion to the 1ML InAs/6ML GaAs superlattice at a substrate temperature of 575°C on top of which a 10nm GaAs section was grown. The temperature was then lowered to 525°C and 10nm of GaAs was grown followed by the second version of the 1ML InAs/3ML GaAs superlattice. [110]-oriented specimens were prepared using the conventional cross-section technique and were finished with a low energy ion mill at 400eV and at an angle of 6°

using a Technoorg GentleMill (Scott et al., 1996). In addition, the Z numbers of Ga, As and In are 31, 33 and 49, respectively.

HAADF images were acquired using the aberration-corrected SuperSTEM 1 microscope. This instrument is based on a VG HB501 100kV STEM that is fitted with a NION Mark II corrector and a Gatan-ENFINA spectrometer for the collection of electron energy loss spectroscopy (EELS) data. HAADF images were acquired using a probe semi-convergence angle of 24mrad and a detector angular range of 70mrad to 210mrad. The image intensity black level was set to give a few image counts per pixel (~5-10) above the noise without any specimen material. Image counts are typically of the order of several thousand in the presence of a specimen. Images were taken from uniform and flat specimen areas. After the acquisition of an image, the probe was scanned rapidly across the entire image area (i.e. both InAs and GaAs layers included) and 50 low loss EELS spectra were averaged. An EELS collection semi-angle of 12mrad was used and an effective Z number was determined by considering the extent of the InAs and GaAs layers present in each image. The method described by Egerton (1996) was then used to obtain a measure of the specimen thickness for a particular image. The presence of any surface damage layers and uncertainty in the estimation of the inelastic mean free path will result in an error in the thickness measurements. However, the error is not significant enough to prevent a close agreement between simulation and experiment for bulk GaAs column ratio values as discussed below.

The HAADF images were converted into maps of the dumbbell column ratio which is defined as  $(I_{III} - I_{BD}) / (I_V - I_{BD})$ .  $I_{III}$  and  $I_V$  are the total HAADF signals at the Group III and Group V columns of a particular dumbbell, respectively, and  $I_{BD}$  is the background signal for each column in the dumbbell. The automated image processing technique that was employed is described in detail by Robb and Craven (2008) and Robb et al. (2012). In the first step of the process, an image sub-section around a dumbbell is identified and a variable reference area is overlaid and compared. The reference area consists of Gaussians that describe the expected size, shape and separation of the column intensities within a dumbbell. Optimum reference parameters are chosen to generate the maximum correlation coefficient between the dumbbell image subsection and the reference Gaussians. In this way, the location of the column intensities is established for a particular dumbbell. The values of  $I_{III}$  and  $I_V$  are then measured by integrating over  $3 \times 3$  pixels to reduce the effect of noise. A similar method using inverted Gaussians is used to measure the minimum background positions around a dumbbell

to determine  $I_{BD}$ . The column ratio is then calculated and the same process is performed for every dumbbell (and background position) in the image through the use of translation vectors to move from one dumbbell to the next. A map of the column ratio values is then generated.

Frozen-phonon multislice code modified from Kirkland (1998) was used to perform HAADF STEM calculations of the column ratio of bulk InAs, bulk GaAs and across a perfect InAs/GaAs interface. The supercell for each bulk material was composed of  $16 \times 16$  [110]-unit cells and was constructed from  $2048 \times 2048$  pixels for adequate sampling in real and reciprocal space. The bulk InAs and bulk GaAs supercells had a slice thickness of  $2.14 \text{ \AA}$  and  $2.0 \text{ \AA}$ , respectively, and the column ratio was calculated at each slice thickness up to  $100 \text{ nm}$  (500 slices). The InAs/GaAs interface supercell was composed of  $8 \times 16$  [110]-unit cells of InAs joined to  $8 \times 16$  [110]-unit cells of GaAs without any strain with a slice thickness of  $2.14 \text{ \AA}$ . The column ratio was calculated for 16 dumbbells across the centre of the interface supercell at thicknesses of  $5 \text{ nm}$ ,  $15 \text{ nm}$  and  $30 \text{ nm}$ . Simulated parameters were chosen to match the SuperSTEM 1 probe and the experimental conditions. The simulated probe was formed using an accelerating voltage of  $100 \text{ kV}$ , a convergence semi-angle of  $24 \text{ mrad}$  and aberration coefficients up to and including  $C_{5,6}$  (6-fold astigmatism of  $C_5$ ). The HAADF detector angles also matched those of SuperSTEM 1. To simulate the effect of thermal vibrations on the HAADF signal, the Einstein model for phonon vibrations was implemented at a temperature of  $300 \text{ K}$  and 100 phonon configurations were averaged for each probe position. The Debye-Waller factors and atomic displacements for the atoms in GaAs and InAs were taken from Reid (1983). 100 phonon configurations were chosen to give a smaller standard error in the simulated column ratio values than that measured experimentally ( $\sim 1\text{-}2\%$ ).

### 3. Results and Discussion

Fig. 1(a) shows the simulated column ratio of bulk InAs and bulk GaAs as a function of specimen thickness. The column ratio of InAs has a value greater than one (i.e. the intensity of the In column is greater than that of the As column) for thin crystals as expected from the Z sensitivity of HAADF imaging. The column ratio then drops off rapidly with thickness to reach a value close to 0.85 after a crystal depth of  $\sim 30 \text{ nm}$ . In comparison, the column ratio of GaAs slowly rises to give a constant value of about one at a depth of  $\sim 25 \text{ nm}$ . Overlaid onto the GaAs plot are experimental column ratio values for bulk GaAs. Each experimental data point has a standard error of  $1\text{-}2\%$  and was obtained from averaging over 600 dumbbells.

Similar experimental values were not obtained for bulk InAs due to the difficulty in growing wide layers of bulk InAs. Fig. 1(a) illustrates that there is a good agreement between the simulated and experimental GaAs values showing that the simulations can reproduce the column ratio values observed experimentally sufficiently well and that the error in the experimental thickness measurements is minimal.

Also shown in Fig. 1(a) is the simulated In/Ga ratio which drops below unity at a thickness of  $\sim 24$ nm. This thickness could also be estimated from the intercept point of the InAs and GaAs plots as the As column intensities are uniform across the two materials. Hence, despite the fact that In is heavier than Ga, In columns only appear more intense than Ga columns below this critical thickness. This is a result of the probe being completely de-channelled at lower depths along In columns in contrast to the lighter Ga columns. However, layers of higher Z material will still appear more intense in an image due to the generation of a higher background signal which does not provide high-spatial resolution information. In the case of InAs and GaAs, it is clear that under some conditions the two materials will be difficult to distinguish using the column intensities. Thus, knowledge of the specimen thickness is essential for the interpretation of HAADF images and column ratio analysis.

Simulated column ratio profiles across the perfect InAs/GaAs interface are provided in Fig. 1(b) at thicknesses of 5nm, 15nm and 30nm. For each thickness, the bulk values of InAs and GaAs are indicated by the straight lines on either side of the interface. It is clear that the column ratio values are consistent with bulk values at all thicknesses and they are therefore not altered by the generation of a modified background signal due to the presence of the perfect interface. Hence, any measured non-sharpness will be the result of compositional mixing and not due to probe spreading across a perfectly abrupt interface.

Fig. 2(a) presents a HAADF image of the 1ML InAs/6ML GaAs superlattice with regions of bulk GaAs on either side. The specimen thickness was measured by EELS to be  $\sim 15$ nm. The column ratio of InAs and GaAs should therefore be about 1.15 and 0.95, respectively, from the simulations. A magnified image section is shown in the inset of Fig. 2(a) with a schematic of the dumbbell structure overlaid. Column ratio analysis was performed over the rectangle section highlighted in Fig. 2(a). The column ratio of every dumbbell in the section was measured and the relative positions of the dumbbells replicated in a chess-board distribution

along the  $[001]$  (x) and  $[1\bar{1}0]$  (y) directions to generate a column ratio map. Fig. 2(b) illustrates the column ratio map with a greyscale range of 0.95 to 1.15. The distribution of local composition, obtained from the high-spatial resolution column intensities, is now apparent with the brightest dumbbells most InAs-like and the darkest dumbbells most GaAs-like. Hence, Fig. 2(b) essentially displays a map of the In concentration of each column across the superlattice.

It is evident from Fig. 2(b) that the periodicity of the superlattice is present with clear alternating bands of In and Ga rich regions. However, the composition of the structure is not uniform with variation in the amount of In contained within individual layers and the presence of considerable interfacial roughness. Fig. 2(c) is an averaged column ratio line profile generated from the average value of the dumbbells summed along the y direction. The error bars in Fig. 2(c) are equal to the standard error of each summed dumbbell row. The line profile reveals that each 1ML InAs layer is actually 3-4ML in extent. This is evidence that the In atoms have segregated over 3-4ML across each interface in the superlattice. Furthermore, Fig. 2(c) shows that the experimental column ratio values of the GaAs and InAs are generally consistent with the simulations although the peak value of the InAs layers is ~7% less than that predicted by the simulations. This reduction is due to the segregation of the In atoms that results in columns with a mixture of Ga and In atoms instead of pure In.

Fig. 3 gives a HAADF image of the shorter period 1ML InAs/3ML GaAs superlattices grown at different temperatures. The lower temperature superlattice exhibits a slightly higher contrast in Fig. 3 due to a small difference in the specimen tilt at each superlattice. However, the tilts were optimised for each superlattice before the acquisition of high magnification data. Column ratio analysis was performed over the two rectangle sections highlighted in Fig. 3. Specimen thickness was measured by EELS to be ~15nm for each section. Fig. 4(a) provides the column ratio map of the 525°C grown superlattice. In this case, there is a significant interruption in the layer repeats and the existence of the superlattice structure is not at all apparent with significant blurring and compositional mixing. However, the averaged column ratio line profile in Fig. 4(b) highlights the existence of 10 column ratio peaks that are associated with the positions of the InAs layers. This demonstrates that the underlying superlattice periodicity is in fact present but much less well defined than the 1ML InAs/6ML GaAs superlattice. The fact that there is only a small drop in column ratio values between the

InAs peaks also indicates substantial intermixing of the layers. The segregation of the In atoms is therefore much greater than 3-4ML observed for the wider period superlattice.

The column ratio map of the 575°C grown superlattice is provided in Fig. 5(a). In comparison to the lower temperature grown superlattice, the layers of the 575°C grown superlattice are visibly present and much better defined. The averaged column ratio line profile in Fig. 5(b) also demonstrates 10 distinct column ratio peaks. As was the case with the 1ML InAs/6ML GaAs superlattice, the In appears to have segregated over 3-4ML. Since the spacing between the InAs layers is only 3ML, the column ratio values do not quite drop to bulk GaAs values in these areas. The reason for the better quality of the higher temperature superlattice is likely due to the fact that In atoms tend to clump on top of each other when an In flux is incident on a (relatively) cold surface thereby creating uneven surfaces. In contrast, In atoms that impinge upon a (relatively) warm surface tend to reposition themselves more evenly producing sharper interfaces. However, if the temperature is too high then a greater diffusion of the In atoms will degrade the interfaces. Nevertheless, it is apparent that the growth temperature has a substantial effect on layer quality and it is reasonable to assume that InAs/GaAs based structures can be improved through the fine-tuning of the MBE growth conditions. It is also clear that changes in the quality of the layers can be detected and distinguished at the atomic-scale using column ratio analysis which could compliment the analysis of In segregation by existing numerical methods.

#### **4. Conclusions**

It was demonstrated that the level of In segregation in short period InAs/GaAs superlattices can be detected by the method of column ratio mapping applied to aberration-corrected HAADF images. Simulations of the column ratio were also performed in order to improve the interpretation of experimental column ratio values. The simulations revealed that In columns only appear more intense than Ga columns below a certain specimen thickness and the InAs column ratio decreases rapidly with thickness. Simulations across a perfect InAs/GaAs interface also showed that any perceived non-sharpness in the experimental analysis is the result of real compositional changes and not due to probe spreading. The experimental analysis established that the MBE growth technique is capable of growing InAs based multilayers that incorporate ultra-thin layers of InAs and GaAs. This is regardless of the tendency of In to segregate into surrounding layers over a range of 3-4ML. The effect of

substrate temperature on the quality of the narrower 1ML InAs/3ML GaAs superlattice was also illustrated with the higher temperature producing a higher quality structure.

## **Acknowledgements**

This work was funded by the Engineering and Physical Sciences Research Council under grants GR/S41036/01 and EP/F002610/1 with support for one of the authors (MF) from the Doctoral Training Account. We are grateful to Martin Holland for growing the MBE materials and to Brian Miller for specimen preparation. We would also like to thank Andrew Bleloch, Mhairi Gass, Uwe Falke and Meiken Falke for SuperSTEM technical support and advice.

## **Figure captions**

Fig. 1. (a) Simulated column ratio for bulk InAs and bulk GaAs as a function of specimen thickness. Also shown is the simulated column ratio for In/Ga. Experimental column ratio values of bulk GaAs are overlaid. (b) Simulated column ratio profiles across the perfect InAs/GaAs interface at thicknesses of 5nm, 15nm and 30nm.

Fig. 2. (a) HAADF image of the 6 repeat 1ML InAs/6ML GaAs superlattice. The rectangle section highlights the area of column ratio analysis. The inset provides a magnified image section with the dumbbell structure overlaid. (b) Column ratio map of the superlattice taken from the highlighted section in (a). (c) Column ratio profile averaged over the column ratio map in (b).

Fig. 3. HAADF image of the 10 repeat 1ML InAs/3ML GaAs superlattices grown at 525°C and 575°C. Column ratio analysis was performed over each rectangle section.

Fig. 4. (a) Column ratio map of the 10 repeat 1ML InAs/3ML GaAs superlattice grown at 525°C taken from the rectangle section in Fig. 3. (b) Column ratio profile averaged over the column ratio map in (a).

Fig. 5. (a) Column ratio map of the 10 repeat 1ML InAs/3ML GaAs superlattice grown at 575°C taken from the rectangle section in Fig. 3. (b) Column ratio profile averaged over the column ratio map in (a).

## Reference

Cheng, K.Y., 1997. Molecular beam epitaxy technology of III-V compound semiconductors for optoelectronic applications. *Proceedings of the IEEE* 85, 1694-1714.

Davies, J.H., 2005. *The physics of low-dimensional semiconductors*, Cambridge University Press.

DiLorenzo, J.V., Lauterwasser, B., Zaitlin, M.P., 1997. Applications of MBE grown PHEMTs. *Journal of Crystal Growth* 175/176, 1-7.

Dwyer, C., Etheridge, J., 2003. Scattering of Å-scale electron probes in silicon. *Ultramicroscopy* 96, 343-360.

Eisele, H., Lenz, A., Hennig, C., Timm, R., Ternes, M., Dahne, M., 2003. Atomic structure of InAs and InGaAs quantum dots determined by cross-sectional scanning tunneling microscopy. *Journal of Crystal Growth* 248, 322–327.

Egerton, R.F., 1996. *Electron energy-loss spectroscopy in the electron microscope*, second ed. Plenum Press.

Fu, L., Li, Q., Kuffner, P., Jolley, G., Gareso, P., Tan, H.H., Jagadish, C., 2008. Two-color InGaAs/GaAs quantum dot infrared photodetectors by selective area interdiffusion. *Applied Physics Letters* 93, 013504.

Hillyard, S., Loane, R.F., Silcox, J., 1993. Annular dark-field imaging: resolution and thickness effects. *Ultramicroscopy* 49, 14-25.

Howe, P., Le Ru, E.C., Murray, R., Jones, T.S., 2005. Indium segregation during multilayer InAs/GaAs(0 0 1) quantum dot formation. *Journal of Crystal Growth* 278, 57–60.

Huang, X., Liu, F., Che, X., Liu, J., Lei, W., 2004. Characterization of InAs quantum dots on lattice-matched InAlGaAs/InP superlattice structures. *Journal of Crystal Growth* 270, 364–369.

Karpov, S.Y., Makarov, Y.N., 2000. Indium segregation kinetics in InGaAs ternary compounds. *Thin Solid Films* 380, 71-74.

Kirkland, E.J., 1998. *Advanced Computing in Electron Microscopy*, Plenum Press, New York.

Kitada, T., Shimomura, S., Hiyamizu, S., 2007. Surface segregation of indium atoms during molecular beam epitaxy of InGaAs/GaAs superlattices on (n11)A GaAs substrates. *Journal of Crystal Growth* 301–302, 172–176.

Klenov, D.O., Stemmer, S., 2006. Contributions to the Contrast in Experimental High-Angle Annular Dark-Field Images. *Ultramicroscopy* 106, 889-901.

Malmkvist, M., Mellberg, A., Rorsman, N., Zirath, H., Grahn, J., 2006. Integration of components in a 50-nm pseudomorphic In<sub>0.65</sub>Ga<sub>0.35</sub>As In<sub>0.40</sub>Al<sub>0.60</sub>As InP HEMT MMIC technology. *Solid-State Electronics* 50, 858-864.

Mozume, T., Gozu, S., 2009. High-resolution X-ray diffraction analysis of InGaAs/AlAsSb coupled double quantum wells grown by molecular beam epitaxy. *Journal of Crystal Growth* 311, 1707–1710.

Noda, T.T., Sumidab, N., Koshibab, S., Nishiokab, S., Negib, Y., Okunishic, E., Akiyamaa, Y., Sakakia, H., 2005. STEM studies of MBE-grown corrugated structures of GaAs, InGaAs and AlAs on (7 5 7)B substrates. *Journal of Crystal Growth* 278, 569-574.

Pennycook, S.J., Jesson, D.E., 1991. High-resolution Z-contrast imaging of crystals. *Ultramicroscopy* 37, 14-38.

Pennycook, S.J., Jesson, D. E., 1990. High-resolution incoherent imaging of crystals. *Physical Review Letters* 64, 938-941.

Rebohle, L., Schreya, F.F., Hofera, S., Strassera, G., Unterrainer, K., 2003. Energy level engineering in InAs quantum dot stacks embedded in AlAs / GaAs superlattices. *Physics Review E* 17, 42-45.

Reid, J.S., 1983. Debye-Waller factors of zinc-blende structure materials- a lattice dynamical comparison. *Acta Crystallographica* A39, 1-13.

Robb, P.D., Finnie, M., Longo, P., Craven, A.J., 2012. Experimental evaluation of interfaces using atomic-resolution high angle annular dark field (HAADF) imaging. *Ultramicroscopy* 114, 11-19.

Robb, P.D., Craven, A.J., 2008. Column ratio mapping: A processing technique for atomic resolution high-angle annular dark-field (HAADF) images. *Ultramicroscopy* 109, 61-69.

Rossouw, C.J., 2003. Channelling effects in atomic resolution STEM. *Ultramicroscopy* 96, 299-312.

Scott, C.P., Craven, A.J., Hatto, P., Davies, C., 1996. TEM cross-section preparation with minimal ion milling time. *Journal of Microscopy* 182, 186-191.

Sze, S.M., 2002. *Semiconductor devices: physics and technology*, John Wiley & Sons.

**Figure**

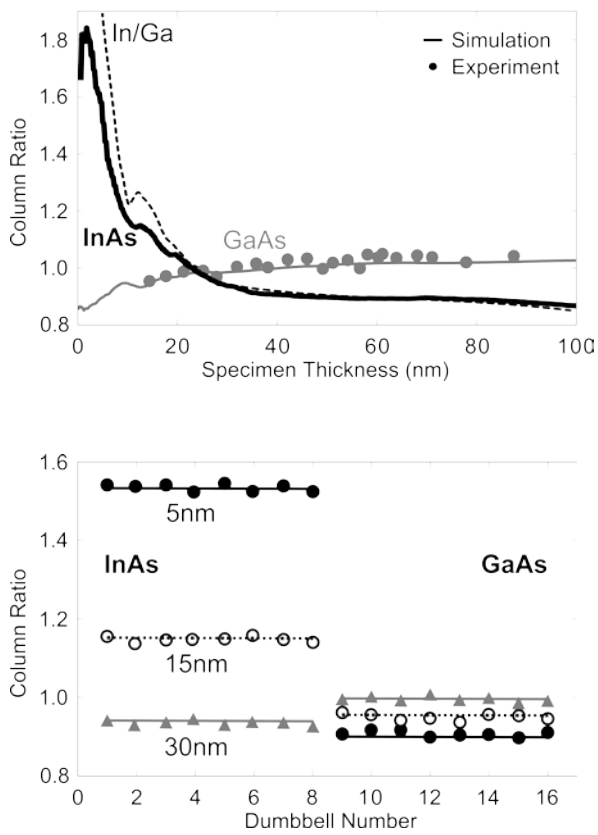


Fig. 1. (a) Simulated column ratio for bulk InAs and bulk GaAs as a function of specimen thickness. Also shown is the simulated column ratio for In/Ga. Experimental column ratio values of bulk GaAs are overlaid. (b) Simulated column ratio profiles across the perfect InAs/GaAs interface at thicknesses of 5nm, 15nm and 30nm.

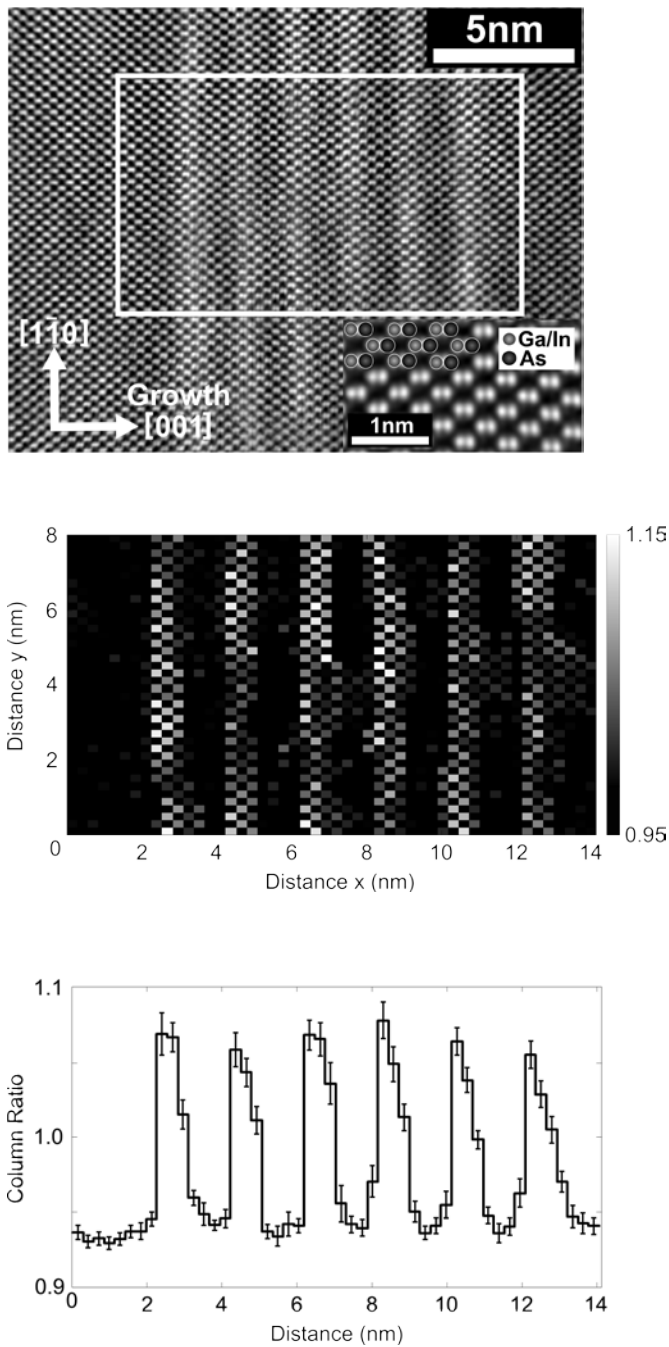


Fig. 2. (a) HAADF image of the 6 repeat 1ML InAs/6ML GaAs superlattice. The rectangle section highlights the area of column ratio analysis. The inset provides a magnified image section with the dumbbell structure overlaid. (b) Column ratio map of the superlattice taken from the highlighted section in (a). (c) Column ratio profile averaged over the column ratio map in (b).

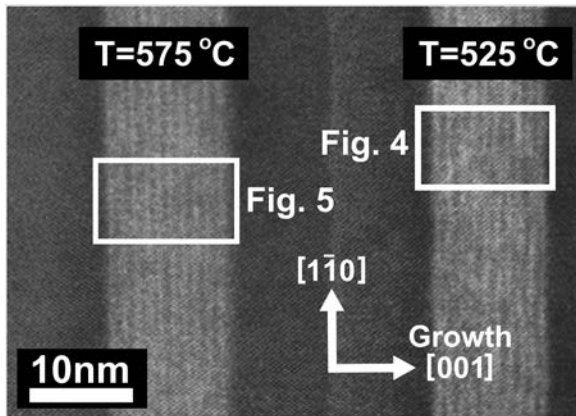


Fig. 3. HAADF image of the 10 repeat 1ML InAs/3ML GaAs superlattices grown at  $525^{\circ}\text{C}$  and  $575^{\circ}\text{C}$ . Column ratio analysis was performed over each rectangle section.

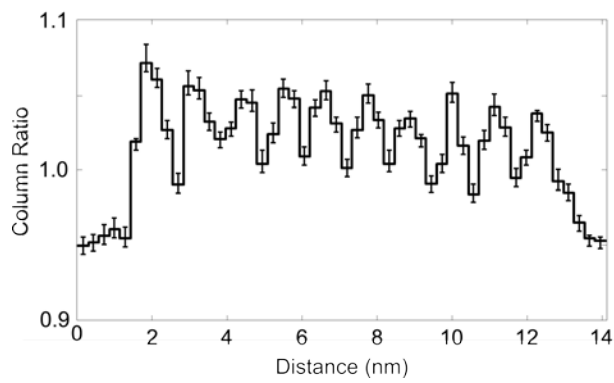
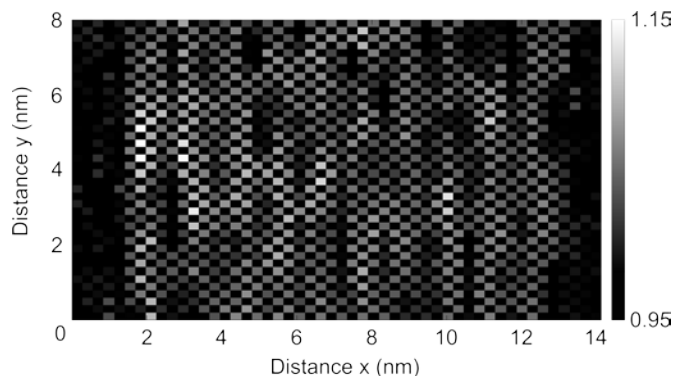


Fig. 4. (a) Column ratio map of the 10 repeat 1ML InAs/3ML GaAs superlattice grown at 525°C taken from the rectangle section in Fig. 3. (b) Column ratio profile averaged over the column ratio map in (a).

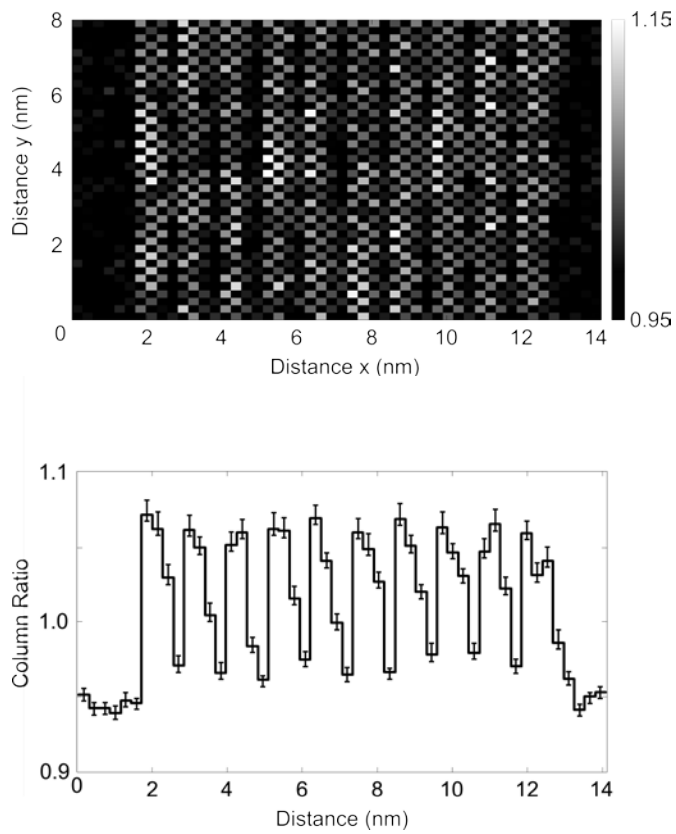


Fig. 5. (a) Column ratio map of the 10 repeat 1ML InAs/3ML GaAs superlattice grown at  $575^{\circ}\text{C}$  taken from the rectangle section in Fig. 3. (b) Column ratio profile averaged over the column ratio map in (a).